Liquid flow induced by ion evaporation in an electrified meniscus

F. J. Higuera
E. T. S. Ingenieros Aeronáuticos, Plaza Cardenal Cisneros 3, 28040 Madrid, Spain
(Received 11 November 2003; revised manuscript received 30 January 2004; published 2 June 2004)

A simple model is proposed for the flow around the apex of a meniscus of a liquid undergoing ion evaporation in a vacuum under the action of a high electric field. The model includes a simplified description of the effect of the space charge surrounding the evaporating surface, and the idealizations that ion evaporation occurs at a constant surface field and that the electric field and viscous forces are negligible in the liquid. In agreement with known experimental and theoretical results for liquid metal ion sources, numerical solutions of the model problem show that the meniscus develops a protrusion and the current-voltage characteristic is linear in a range of voltages above an extinction voltage at which evaporation switches off. An oscillatory regime and transient evolutions ending in surface pinch-off and the emission of a drop are described, and the stabilizing effect of the pressure variations due to the evaporation flux is discussed. Asymptotic estimates for large evaporation flow rates are worked out.

DOI: 10.1103/PhysRevE.69.066301 PACS number(s): 47.65.+a

I. INTRODUCTION

A liquid metal ion source (LMIS) is a device in which ions of a metal are emitted from a meniscus of the liquefied metal held in a vacuum and stressed by a high electric field due to a voltage applied between the meniscus and another electrode. Away from its apex, the meniscus takes the form of a Taylor cone [1], which is an equilibrium shape reflecting the hydrostatic balance of surface tension and electric stresses. Ion emission occurs by field evaporation [2] from a small region of high field around the apex, which is surrounded by a high space charge. The space charge tends to reduce the field at the surface, but this tendency is offset by a deformation of the meniscus, which departs from a cone in the vicinity of the apex and develops a characteristic protrusion capped by the emitting region. The source emits ions and clusters in various charge stages, accompanied by a fraction of neutrals, mainly as microdroplets, which increases when the voltage and the current increase. LMIS's find application in the general area of microfabrication, as well as in microscopy and materials analysis and implantation. Work carried out in this field prior to 1991 was summarized by Prewett and Mair [3], and a review of the basic physics of a LMIS has been given by Forbes [4].

More recently, ion emission from Taylor cones of dielectric liquids has been investigated as a means to enlarge the ranges of chemical composition and mass/charge of the ions, and thus the range of applications [5]. To name two examples, values of mass/charge well above the 200 Da attainable with a LMIS are of interest in electrical propulsion to reduce the energy consumed per unit thrust; and a simple and efficient source of large and fragile ions of biomolecules would be of much interest for mass spectrometry. The fact that field evaporation of ions is the relevant process also for dielectric liquid was proposed by Iribarne and Thomson [6] and confirmed by a number of researchers [5,7]. A mixed drops-and-ions regime, in which most of the mass is carried by charged drops but a noticeable fraction of the electric current is carried by ions, was found by Gamero-Castaño *et al.* [5]. Further work by these authors and by Romero-Sanz *et al.* [8] has shown that a pure ionic regime can be approached or reached with organic solvents such as formamide or propylene carbonate, and with ionic liquids, which are purely ionic materials in the liquid state with electric conductivities of $1-10\ \mathrm{S/m}$. Experiments with some of these liquids have revealed narrow energy distributions of the ions, similar to those of a LMIS.

The protrusion at the tip of the meniscus of a LMIS was first observed by Aitken [9] in a caesium source using a scanning electron microscope, and by Gaubi *et al.* [10] and Benassayag *et al.* [11] in gallium sources using a transmission electron microscope. This protrusion is often termed the cusp, probably due to its appearance in electron microscope micrographs, though it is recognized that the actual surface may be rounded at the end of the cusp. The length of the cusp was seen to increase with the emission current. Kingham and Swanson [12] introduced a model of a LMIS consisting of a jetlike protrusion on the end of a cone. Using a self-consistent evaluation of the effect of the space charge and a simplified fluid dynamical model, these authors numerically computed approximations to the current-voltage characteristic and the length of the protrusion. Further work along these lines was carried out by Forbes and co-workers [13], who improved the modeling of the surface shape and obtained lengths of the protrusion in better agreement with transmission electron microscope experiments. Mair [14] (see also Refs. [15,16]) theoretically determined the current-voltage characteristic on the basis of an equilibrium of the electric and surface tension forces acting on the whole meniscus. The fluxes of mass and momentum carried by the evaporating liquid are neglected in this theoretical model; the effect of the space charge is accounted for by means of an approximation that gives the emission current in terms of the difference between the actual electric force and the electric force in the absence of space charge (see Sec. II A below); and the latter force is computed by linearizing the voltage about the extinction voltage at which the source switches off. The result is a linear current-voltage relationship with a slope which is in good agreement with experiments for viscous-drag-free sources. Analytical approximations for the length

of the protrusion and the curvature radius of the surface at the apex were worked out by Mair and Forbes [17] combining these results with Vladimirov and Gorshkov's [18] expression of the harmonic field at the apex of the protrusion, in an analysis that takes into account the depression due to the flow induced in the liquid by ion evaporation. Mair and Forbes's theory leads to a linear relationship between the length of the protrusion and the emission current.

The transient response and the instability of a LMIS are also of much interest. The fast current oscillations that are observed when a source is operated at high current have been attributed to hydrodynamic instabilities of the cusp or of a part of the cone, which may lead to the emission of microdroplets (Mair and Engel [19], Prewett and Mair [3]). Indirect evidence of vibrations of the tip of the cone has been given by Gaubi *et al.* [10], while Bar and Brown [20] and Praprotnik *et al.* [21] observed microdroplets emitted by the meniscus. Mair [22] presented a simple theoretical model of the bulk oscillations of a conical meniscus subject to surface tension and electric stress, and Vladimirov *et al.* [23] discussed the capillary waves at the surface of the liquid. Preliminary numerical computations of a nonstationary LMIS have been carried out by Zheng and Linsu [24] and Forbes *et al.* [16].

In this paper, numerical computations and order-of-magnitude estimates are presented for the stationary state and transient evolution of the surface of a liquid ion source in the vicinity of its apex. The viscosity of the liquid is neglected, which is an assumption often used in the analysis of LMIS's. The assumption is marginally valid for some dielectric liquids but not for ionic liquids, which are very viscous at ambient temperature. The electric conductivity of the liquid is taken to be infinitely large, which is also an approximation more suitable for metallic liquids than for other liquids undergoing ion evaporation. Attention is restricted to a region around the apex including the protrusion and a part of the cone. This region is assumed to be small compared with the size of the meniscus, the distance to the extractor electrode, and any other length of the system. Boundary conditions at the outer boundary of this region express its matching to more remote regions which need not be analyzed in detail. The evolution of interest is associated to the dynamics of the liquid, which is slow compared with the response of the space charge around the evaporating surface. The distribution of space charge is therefore assumed to be quasisteady, and its description is further simplified by adopting, as a model, the results of a unidimensional analysis, as has been done before by Mair and co-workers [14,15,17]. The sensitivity of the current evaporation rate to the electric field is taken to be infinitely high, which leads to a constant (maximum) field at the evaporating region of the surface and zero evaporation current in the rest of the surface.

A current-voltage characteristic featuring an extinction voltage and an ample range of linear increase of the current with the voltage is obtained, in agreement with existing theoretical and experimental results. An asymptotic description of the stationary solution for large voltages is also given. The numerical results show the stabilizing effect of the liquid flow induced by ion evaporation. In the absence of the depression due to this flow, the surface elongates continuously and appears to shed drops (though a complete description of the shedding process is not attempted here). The evaporation-induced depression stabilizes the surface, confining the oscillations of the tip and the emission of drops to large values of the voltage, and some times also to a range of voltages immediately above extinction.

II. FORMULATION

A. Model problem for the space charge

Ion evaporation from the surface of a liquid metal [2,25] or a liquid of high electrical permittivity [6] in a vacuum is characterized by a density of current across the surface that is a rapidly increasing function of the electric field. In a continuum Eulerian description, the density and velocity of the space charge, n_{sc} and $\boldsymbol{v}_{sc}$, and the negative of the electric potential, φ with $\boldsymbol{E}=\boldsymbol{\nabla}\varphi$, obey

$$\nabla^2\varphi = \frac{qn_{sc}}{\epsilon_0}, \tag{1a}$$

$$\boldsymbol{\nabla}\cdot(n_{sc}\boldsymbol{v}_{sc}) = 0, \tag{1b}$$

$$\boldsymbol{v}_{sc}\cdot\boldsymbol{\nabla}\,\boldsymbol{v}_{sc} = \frac{q}{m}\boldsymbol{\nabla}\,\varphi, \tag{1c}$$

$$\boldsymbol{x}\in\Sigma_l\colon\ \varphi = 0, \quad \boldsymbol{v}_{sc} = 0, \quad j \equiv qn_{sc}\boldsymbol{v}_{sc}\cdot\boldsymbol{n} = f(|\boldsymbol{\nabla}\varphi|), \tag{2}$$

plus additional conditions for the electric potential at other boundaries of the system. Here Σ_l is the surface of the liquid, of outer normal $\boldsymbol{n}$, m and q are the mass and charge of the evaporated ions, ϵ_0 is the permittivity of vacuum, and j is the density of evaporation current. The distribution of space charge is assumed to be quasisteady, which is appropriate for the analysis of the relatively slow response of the liquid.

The strong sensitivity of the evaporation current density j with the electric field often leads to a space-charge controlled regime in which the density of space charge is high around the high field regions of the surface, screening the surface and preventing a further increase of the field. In these conditions, the field is nearly a constant in the evaporating region of the surface, at a value E_0 that is evaluated in what follows, and the evaporation current density is negligible where the surface field is smaller than E_0. Let L be the characteristic size of the evaporating region. The characteristic velocity of the space charge in this region is $v_c = \sqrt{(q/m)E_0L}$, from Eq. (1c), and the space-charge density is of the order of $n_c = f(E_0)/qv_c$, from the third condition (2). The electric field induced by the space charge is of order qn_cL/ϵ_0, from Eq. (1a), and the condition that this field should be of the order of the field at the surface (E_0) in order for the effect of the space charge to matter, gives finally $f(E_0)/E_0^{3/2} = \epsilon_0(q/m)^{1/2}/L^{1/2}$.This result depends on the characteristic length L, but the dependence is very weak; it is only logarithmic in the usual case in which the function f involves an exponential. Then, calling $\chi = (E\,d\ln f/dE|_{E_0}$

$\gg 1$, the evaporation law can be approximated by $f(E) = f(E_0)\exp\{\chi(E/E_0-1)\}$. In the asymptotic limit $\chi\to\infty$, conditions (2) become

$$\boldsymbol{x}\in\Sigma_l:\begin{cases}\varphi=0, \quad \boldsymbol{v}_{sc}=0,\\ |\boldsymbol{\nabla}\varphi|=E_0 \quad \text{at the evaporating region}\\ j=0 \text{ at the nonevaporating region } (|\boldsymbol{\nabla}\varphi|<E_0).\end{cases} \tag{3}$$

The two conditions that $\varphi=0$ and $|\boldsymbol{\nabla}\varphi|=E_0$ determine j in the evaporating region.

Problem (1), (3) has a well known solution for the case of a plane evaporating surface at a distance L from a plane parallel electrode kept at a voltage V relative to the surface [26]. For small values of $(V-V_0)/V_0$, where $V_0=E_0L$, this solution gives

$$j=\frac{3}{8}\varepsilon_0\sqrt{\frac{2q/m}{E_0L}}(E_h^2-E_0^2), \tag{4}$$

where $E_h=V/L$ is the harmonic field that would exist at the evaporating surface in the absence of space charge. Mair [27] showed that Eq. (4) gives a reasonable approximation to the evaporation current even when the condition $(V-V_0)/V_0 \ll 1$ is not satisfied and, moreover, that geometry has no particularly strong effect on the space-charge reduction of the surface field. This means that a relation of the type (4) with the coefficient of $(E_h^2-E_0^2)$ changed to an adjustable value provides an approximation to the solution of Eqs. (1) and (3) for liquid surfaces more complex than a plane. The approximation has been used in different problems [28], in particular for an approximate determination of the current-voltage characteristic [14–16] and the surface shape [17] of a LMIS. It will be adopted in what follows as a simplified model of the space charge.

To summarize, problem (1), (3) is replaced by the following model problem:

$$j=\max\{\alpha(E_h^2-E_0^2),0\}, \tag{5}$$

where α is a model constant and the harmonic field is given by $E_h=|\boldsymbol{\nabla}\varphi_h|$ at the surface, with

$$\nabla^2\varphi_h=0 \quad \text{in the vacuum}, \tag{6}$$

$$\varphi_h=0 \quad \text{at the liquid surface}, \tag{7}$$

and additional conditions at the other boundaries, to be discussed below. Once the harmonic field is computed, the field acting on the surface, which is required to evaluate the electric stress (equal to $\frac{1}{2}\varepsilon_0E_n^2$; see, e.g., Ref. [29]), is taken to be

$$E_n=\min(E_h,E_0). \tag{8}$$

B. Flow of the liquid

The contributions of the surface tension and the normal electric stress are both important in the balance of stresses at the surface of a liquid undergoing ion evaporation. The condition that these two contributions are of the same order, namely that $\gamma\boldsymbol{\nabla}\cdot\boldsymbol{n}\sim\frac{1}{2}\epsilon_0E_n^2$, where γ is the surface tension of the liquid and E_n is the electric field normal to its surface, equal to E_0 at the evaporating cap, determines the characteristic curvature radius of the cap as $R_0=\gamma/\epsilon_0E_0^2$ (see Ref. [30]). The velocity v of the liquid in the cap can be estimated from this R_0 and typical values of the total evaporation current $I\sim(q/m)\rho vR_0^2$, where ρ is the density of the liquid. Thus, for a gallium LMIS ($\gamma=7.2\times10^{-1}$ N/m, $E_0\sim15$–20 V/nm, $\rho=5910$ kg/m^3, and $m/q=7.24\times10^{-7}$ kg/C), R_0 is of the order of a few nanometers and the velocity of the liquid is of the order of 10^3 m/s when the source is operated at an evaporation current of 20 μA. The Reynolds number of the liquid flow is then about 10 and thus, insofar as a continuum treatment is admissible, the effect of the viscosity should not be very important and can be neglected as a first approximation. Similar estimates for formamide seeded with NaI ($\gamma=5.8\times10^{-2}$ N/m, $E_0\sim1$ V/nm, $\rho=1133$ kg/m^3, and $m/q=3\times10^{-6}$ kg/C) give a R_0 of the order of 10 nm, whereas the measured flow rate Q, of the order of 10^{-13} m^3/s when the ionic regime is approached, requires velocities of the order of 500 m/s (from $Q\sim vR_0^2$). The Reynolds number is then about 2.

The electric field needed in the liquid to conduct the electric current to the evaporating surface is always small compared with E_0 in the case of liquid metals, which justifies the assumption of an equipotential liquid surface used in Eq. (7) to model the effect of the space charge. For formamide, this assumption is less well justified, because the field required in the liquid may be about one-third of E_0 when a conductivity of 1 S/m, which is typical of some experiments [5], is assumed.

Leaving out the effect of the viscosity, the flow of the liquid will be irrotational, with a velocity $\boldsymbol{v}=\boldsymbol{\nabla}\phi$ and

$$\nabla^2\phi=0 \quad \text{in the liquid}. \tag{9}$$

The surface of the liquid, Σ_l, of equation $f_l(\boldsymbol{x},t)=0$ say (with $f_l<0$ in the liquid), is to be determined as part of the solution using the condition that the mass flux across the surface due to ion evaporation is $(m/q)j$, with j given by Eq. (5). This condition can be written in the form

$$\frac{\partial f_l}{\partial t}+(\boldsymbol{\nabla}\phi-v_e\boldsymbol{n})\cdot\boldsymbol{\nabla}f_l=0, \quad \text{where}$$

$$v_e=\max\{\tilde{\alpha}(E_h^2-E_0^2),0\}, \quad \tilde{\alpha}=\frac{m}{q}\frac{\alpha}{\rho}, \quad \boldsymbol{n}=\frac{\boldsymbol{\nabla}f_l}{|\boldsymbol{\nabla}f_l|}. \tag{10}$$

The balance of stresses normal to the surface reads $\gamma\boldsymbol{\nabla}\cdot\boldsymbol{n}+\beta\rho v_e^2=\frac{1}{2}\epsilon_0E_n^2+p$, where the inward stresses on the left hand side are due to the surface tension acting on the curved surface and the recoil or momentum flux picked up by the evaporating ions. Here $\beta=\rho/\rho_0-1$, where ρ_0 is the density at the "electrical surface" of the evaporating liquid [25], where the electric field is E_0. The terms on the right hand side of the balance of stresses are the electric stress and the pressure of the liquid, which satisfies $p/\rho=-\partial\phi/\partial t-\frac{1}{2}|\boldsymbol{\nabla}\phi|^2$ (see, e.g., Ref. [31]). This equation reduces to the Bernoulli equation when the flow is stationary. In the general

case, the pressure can be eliminated from the balance of stresses to obtain the following evolution equation for the velocity potential at the surface:

$$\rho\left(\frac{\partial \phi}{\partial t}+\frac{1}{2}|\nabla \phi|^2\right)=\frac{1}{2}\epsilon_0 E_n^2-\gamma \nabla \cdot \boldsymbol{n}-\beta\rho v_e^2 \quad \text{at } f_l=0. \tag{11}$$

This provides a boundary condition for Eq. (9).

Additional boundary conditions are needed for φ_h, ϕ, and f_l far from the evaporation region. These conditions depend on the configuration of the system where the meniscus is formed, and bring into the problem the influences of the liquid feeding device and the shape and position of the extractor electrode that is used to create the electric field around the meniscus. While these are important features, they are not intrinsic to the evaporation process going on around the tip of the meniscus, which is the subject of this paper. Here, in order to simplify the analysis and keep the results reasonably general though only qualitative, advantage will be taken of the fact that the evaporation region is typically very small compared with the size of the meniscus and the distance to the extractor. Attention will be restricted to a region around the tip large compared with the evaporation region but small compared with any other length of the system. Conditions at the outer boundary of this region stem from the requirement that the meniscus should tend to a Taylor cone far upstream of the tip, where $j=0$ and the pressure becomes negligible in the balance of stresses normal to the surface. A Taylor cone [1] is a classical hydrostatic solution of the problem when this balance reduces to $\gamma\nabla\cdot\boldsymbol{n}=\frac{1}{2}\epsilon_0 E_n^2$. In this solution, the surface of the liquid is a cone of half angle $\omega_T\approx 49.29°$ and the electric potential is given by $\varphi_h=\varphi_T=A\sqrt{\gamma/\epsilon_0}R^{1/2}P_{1/2}(\cos\theta)$, where R is the distance to the apex of the cone, θ is the angle around its axis, measured from the prolongation of the cone, $P_{1/2}$ is Legendre's function of degree $1/2$, and $A\approx 1.3459$.

The velocity potential far upstream of the evaporation region is that of a sink at the apex, given by $\phi=Q/[2\pi R(1-\cos\omega_T)]$, where Q is the evaporation flow rate. The pressure variation due to this sink flow is of order $\rho Q^2/R^4$. When this is included in the balance of stresses, it leads to a correction of the angle of the cone proportional to $1/R^3$ and to a correction of the electric potential proportional to $1/R^{5/2}$.

The following far field conditions are imposed at a sphere of radius $R_\infty \gg R_0$ to account for these asymptotic results,

$$\varphi_h=A\frac{\gamma^{1/2}}{\epsilon_0^{1/2}}R^{1/2}P_{1/2}(\cos\theta)+B\frac{\gamma^{7/2}}{\epsilon_0^{7/2}E_0^6}\frac{F(\theta)}{R^{5/2}} \quad \text{for} \quad 0\leqslant\theta\leqslant\omega_T, \tag{12a}$$

$$\phi=\frac{Q}{2\pi(1-\cos\omega_T)R} \quad \text{with} \quad Q=\int_{\Sigma_l} v_e \mathrm{d}\sigma \quad \text{for} \quad \omega_T\leqslant\theta\leqslant\pi, \tag{12b}$$

$$f_l=\pi-\omega_T-\theta. \tag{12c}$$

Here B is a free parameter intended to reflect the effect of the variation of the voltage applied between the meniscus and a far electrode. The factor $\gamma^{7/2}/\epsilon_0^{7/2}E_0^6$ multiplying B is introduced for convenience, to make B dimensionless. The function $F(\theta)$ should be given by an expansion in negative powers of R_∞, with a leading term proportional to $P_{-n}(\cos\theta)$, $n\approx 5/2$, if the apparent apex of the cone were to stay at the center of the outer sphere ($R=0$) for any value of B. This condition, however, is difficult to enforce, and it would require to include small corrections also in ϕ and f_l in Eqs. (12b) and (12c). It proves to be simpler to leave Eqs. (12a)–(12c) as they are and allow for a shift of the apparent apex and other small variations of the surface when B is changed. Taking this view, the function $F(\theta)$ in Eq. (12a) can be chosen freely; it will be set to $F(\theta)=\max[P_{-5/2}(\cos\theta),0]$ in what follows. The procedure can be thought of as if the outer boundary $R=R_\infty$ were a real spherical electrode of radius R_∞ with a nonuniform voltage equal to φ_h in Eq. (12a).

This completes the formulation of the problem, which consists of Eqs. (6)–(12). This problem can be rewritten in nondimensional variables by scaling distances, velocities, flow rates, and electric fields with

$$R_0=\frac{\gamma}{\epsilon_0 E_0^2}, \quad v_0=\left(\frac{\gamma}{\rho R_0}\right)^{1/2}=\frac{\epsilon_0^{1/2}E_0}{\rho^{1/2}},$$

$$Q_0=v_0R_0^2, \quad \text{and} \quad E_0, \tag{13}$$

respectively, and measuring the time with R_0/v_0. The velocity scale v_0 represents the velocity that the liquid should have in a region of size R_0 around the apex in order for the dynamic pressure $\rho v_0^2/2$ to be of the same order as the surface tension and the normal electric stress in this region. The actual velocity of the liquid depends on the model parameter $\tilde{\alpha}$. The nondimensional problem coincides with (6)–(12) with the parameters ϵ_0, ρ, γ, and E_0 set to the unity and $\tilde{\alpha}$ in Eq. (10) replaced by

$$\hat{\alpha}=\frac{\tilde{\alpha}E_0^2}{v_0}=\frac{m}{q}\frac{\alpha E_0}{\epsilon_0^{1/2}\rho^{1/2}}, \tag{14}$$

which, along with β and B, are the only dimensionless parameters of the problem (leaving apart R_∞/R_0, which is an artificial parameter whose value should not affect the solution in the evaporation region other than by setting a scale for B, provided R_∞/R_0 is sufficiently large).

III. RESULTS

A. Numerical method

Axisymmetric solutions of (6)–(12) have been computed numerically. For this purpose, the surface of the liquid is discretized using markers ($\boldsymbol{x}_i$). The equations of motion of these markers and of the values of the velocity potential that they carry (ϕ_i) are, from Eqs. (10) and (11),

$$\frac{d\boldsymbol{x}_i}{dt} = \boldsymbol{\nabla}\phi - v_e\boldsymbol{n},$$

$$\rho\frac{d\phi_i}{dt} = \rho\left(\frac{1}{2}|\boldsymbol{\nabla}\phi|^2 - v_e\boldsymbol{n}\cdot\boldsymbol{\nabla}\phi\right) + \frac{1}{2}\epsilon_0 E_n^2 - \gamma\boldsymbol{\nabla}\cdot\boldsymbol{n} - \beta\rho v_e^2. \tag{15}$$

The fields φ_h and ϕ are needed to evaluate the right hand sides of these equations. They are obtained from boundary element solutions of Eqs. (6) and (9) computed using as nodes the markers and a set of fixed equispaced points on the outer spherical boundary. The method is fairly standard and the implementation used here follows that of Oguz and Prosperetti [32].

B. Numerical results

1. Case $\hat{\alpha}=0$

The mass flux accompanying the evaporation of ions [proportional to v_e in Eq. (10)] and the recoil term proportional to v_e^2 in Eq. (11) are suppressed when $\hat{\alpha}=0$. In this case the dynamics are controlled by surface tension and electric forces only. The evaporation of ions does not directly induce a flow in the liquid, but it still affects the solution through its influence on the electric stress $\frac{1}{2}\epsilon_0 E_n^2$ in Eq. (11). In the absence of ion evaporation, the surface field E_n equals the harmonic field $E_h=|\boldsymbol{\nabla}\varphi_h|$, given by the solution of Eq. (6), and satisfies $E_n<E_0$ everywhere on the surface. Evaporation begins when the maximum value of the surface field attains E_0, and it prevents any further increase of the surface field above E_0. In a solution with ion evaporation, the surface field is equal to E_0 in the evaporating region of the surface (to be determined as part of the solution) and smaller than E_0 in the rest of the surface.

The dynamic pressure due to the flow induced in the liquid by ion evaporation has been estimated in the literature for gallium and other LMIS's at low emission currents (about 2 μA in Ref. [4]). The estimated pressure variation is small compared with surface tension and electric stresses in these conditions, which has brought much attention to the limiting case $\hat{\alpha}=0$. Theoretical models of the stationary current-voltage characteristic have been proposed in which the inertia of the liquid is explicitly left out [14].

Numerical computations for $\hat{\alpha}=0$ show, however, that the solution does not tend to a stationary state with ion evaporation. In these computations the meniscus either evolves toward a rounded shape with no evaporation ($E_h<E_0$ everywhere on the surface) or develops a blob that tends to become a drop in a finite time, as illustrated in Fig. 1. Which of these behaviors is obtained depends on the value of B, which gauges the applied voltage, and for a given B it depends on the initial shape of the meniscus. Some of the initial shapes are similar to the stationary menisci proposed in Refs. [12,17], but the numerical solution still does not tend to a stationary state with ion evaporation.

The computations always fail at a finite time when the surface develops a blob (shortly after the last time displayed in the case of Fig. 1). This is because the code cannot handle the pinch-off of the surface, but there is little doubt that the regime captured is akin to the dripping regime described by Notz and Basaran [33] in the absence of ion evaporation. Since the shedding of drops affects only the vicinity of the apex, the present regime should be more properly named microdripping, after the classification of Cloupeau and Prunet-Foch [34].

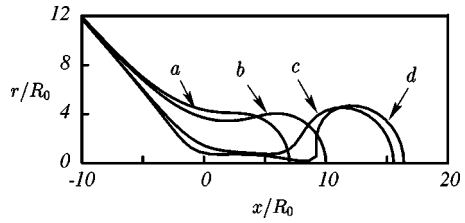

FIG. 1. Time evolution of the meniscus leading to pinch-off for $\hat{\alpha}=\beta=B=0$. Displayed are the surfaces at the nondimensional times $t/(R_0/v_0)=20(a)$, 40 (b), 60 (c), and 62 (d). The initial condition is the stationary meniscus for $\hat{\alpha}=0.2$ and $\beta=B=0$. Here x is the distance along the symmetry axis measured from the center of the outer sphere and r is the distance to the symmetry axis.

That the numerical solution never ends in a stationary state with ion evaporation when $\hat{\alpha}=0$ can be understood by noticing that such state, if it exists, is unstable in the framework of the present model of constant evaporation field. In fact, the stationary evaporating surface would be a spherical cap of radius $4\gamma/\epsilon_0 E_0^2$ under the equilibrium of surface tension and electric stresses, and any perturbation that increases the radius of the cap decreases the inward surface tension stress without changing the outward electric stress, which is always equal to $\frac{1}{2}\epsilon_0 E_0^2$. This leads to an unbalanced outward force that tends to increase the radius of the cap further. Similarly, the radius of the cap would continuously decrease in response to a perturbation that decreases it initially.

It is also apparent that the pressure variations due to the evaporation flow, which are suppressed when $\hat{\alpha}$ is set equal to zero, could cure this instability, because when the unbalanced outward force mentioned above begins to elongate the surface, the harmonic field increases at the cap, causing an increase of the evaporation current [cf. Eq. (5)] and the evaporation velocity of the liquid [v_e in Eq. (10)] if $\hat{\alpha}>0$. This leads to an increased depression at the surface and in the bulk of the liquid, via the Bernoulli equation, which may offset the outward force. The recoil term proportional to β in Eq. (11) has a similar effect but, contrary to the flow-induced depression, it acts only at the evaporating surface.

2. Stationary solutions with $\hat{\alpha}>0$

The magnitude of the evaporation-induced depression is controlled by the nondimensional parameter $\hat{\alpha}$ in Eq. (14). It is not straightforward to evaluate $\hat{\alpha}$ because it depends on α, which was introduced in Eq. (5) as a model parameter. An estimation of α can be obtained from Eq. (4) if L is identified with R_0 defined in Eq. (13). For example, for ion sources of both gallium and formamide seeded with NaI, this identification gives values $\hat{\alpha}$ of the order of 0.1, or somewhat larger if the emission of clusters or the solvation of the ions, which

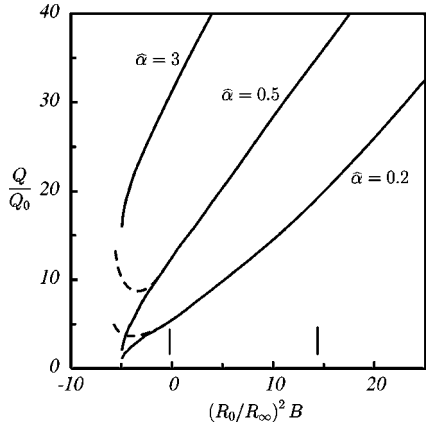

FIG. 2. Nondimensional flow rate (or current) as a function of B for three different values of $\hat{\alpha}$ and $\beta=0$. Solutions computed with different values of R_∞/R_0 lead to nearly identical results when B is scaled with $(R_\infty/R_0)^2$ (see discussion in Sec. III C)

increase the effective mass to charge ratio, are taken into account.

Stationary $(Q/Q_0)-B$ [or $(I/I_0)-B$] characteristics are given in Fig. 2 for three values of $\hat{\alpha}$ and $\beta=0$. Here $I=\rho Q/(m/q)$ is the evaporation current and $I_0=\rho Q_0/(m/q)$. The stationary solutions have been computed using values of R_∞/R_0 that range from 25 to 100. As can be seen, ion evaporation occurs for B above a minimum extinction value. The current increases monotonically with B above the extinction value, and apparently becomes a linear function of B for large values of this parameter. The current also increases with $\hat{\alpha}$ at constant B. Another branch of solutions with a rounded meniscus and no evaporation exists for B below an ignition value which is larger than the extinction value, leading to a region of multiplicity between both values of B. Ignition occurs for $(R_0/R_\infty)^2 B \approx 4$.

The stationary shape of the meniscus in the branch with ion evaporation is represented by the solid curves of Fig. 3 for $\hat{\alpha}=0.2$, $\beta=0$, and three different values of B. For comparison, the dotted curve at the left of this figure shows the rounded meniscus of the frozen solution for $B=0$. (The dashed curve at the right will be commented below.) Figure 4 shows the electric field at the surface and the evaporation

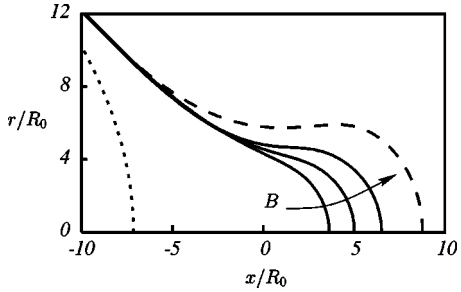

FIG. 3. The solid curves give the stationary shape of the evaporating meniscus for $\hat{\alpha}=0.2$, $\beta=0$, and the three values $(R_0/R_\infty)^2 B=-4.16$, 0, 16, increasing as indicated by the arrow. The dotted curve is the stationary meniscus for $B=0$ in the frozen solution (without ion evaporation). The dashed curve is the stationary meniscus for $\hat{\alpha}=0.2$, $\beta=2$, and $B=0$.

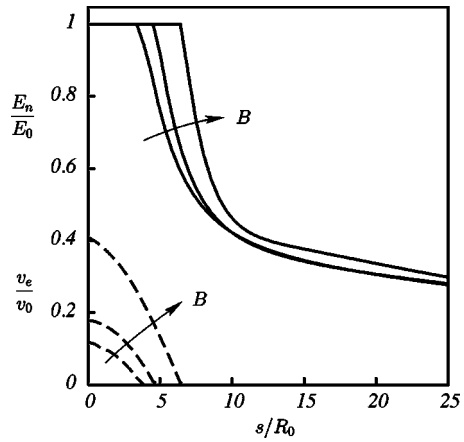

FIG. 4. Nondimensional surface electric field (solid curves) and nondimensional evaporation flux (dashed curves) as functions of the nondimensional arc length measured from the apex along a meridional section of the surface, for the same values of the parameters as in Fig. 4 (B increases as indicated by the arrows).

flux v_e/v_0 as functions of the arc length along a meridional section ($s=0$ at the symmetry axis), and Fig. 5 shows the distributions of electric stress, surface tension, and pressure. The surface always tends to a Taylor cone far upstream, while the tip elongates with increasing B, in agreement with experimental transmission electron microscope observations and theoretical models. The size of the evaporating cap and the maximum evaporation flux, which is attained at the symmetry axis, increase with B. The increase of the latter quantity, however, is only moderate, and it seems to tend to a finite limiting value when B is increased well above the values of Fig. 4. This means that the continuous increase of the current in Fig. 2 is due to the increase of the area of the evaporating cap (see also Sec. III C below). The magnitude of the evaporation-induced depression also increases with B (see Fig. 5). While surface tension is always the dominant inward stress far upstream of the apex, in accordance with Taylor's solution, this needs not be the case around the apex for large values of B. The position of the apex is given in Fig. 6 as a function of the flow rate, and the inverse of the

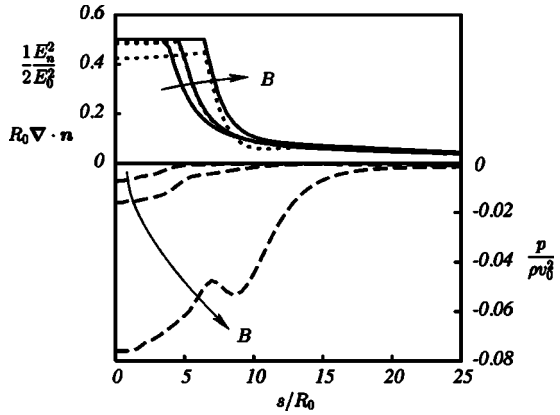

FIG. 5. Nondimensional surface distributions of electric stress (solid), surface tension (dotted), and pressure (dashed, right hand side scale) for the same values of the parameters as in Fig. 4.

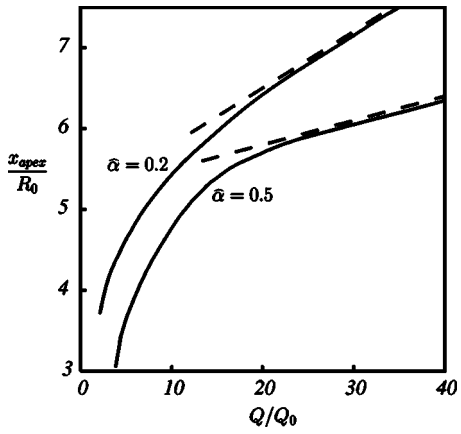

FIG. 6. Axial position of the apex as a function of the flow rate for $\beta=0$ and two values of $\hat{\alpha}$. The dashed straight lines have equations $x_{apex}/R_0=0.07(Q/Q_0)+5.1$ and $x_{apex}/R_0=0.03(Q/Q_0)+5.2$.

mean curvature ($\nabla\cdot\boldsymbol{n}$) of the surface at the apex, which is a measure of the size of the cap, is given in Fig. 7.

3. Effects of the recoil and the far field boundary condition

Solutions with $\beta>0$ (not displayed) show that the effect of the evaporation recoil is to flatten and widen the evaporating cap, which may even develop a neck at its connection to the main meniscus. A sample meniscus for $\hat{\alpha}=0.2$, $\beta=2$, $B=0$ is given by the dashed curve of Fig. 3. Apparently, the recoil cannot stabilize the flow by itself: solutions computed with $\beta>0$ but with the evaporation term proportional to v_e removed from Eq. (10) end up in evaporation shutdown or surface pinch-off, as when $\hat{\alpha}=0$. The recoil may, however, increase the stability of solutions with $\hat{\alpha}>0$.

The particular form of the function $F(\theta)$ used in Eq. (12a) (cf. paragraph following these equations) has a qualitative effect on the (Q/Q_0)–B characteristics in the vicinity of extinction. When this function is replaced by $F(\theta)=P_{-5/2}(\cos\theta)$, the characteristics change as indicated by the dashed curves of Fig. 2. The modified characteristics have not been displayed for positive values of B because there the changes are only quantitative relative to the original characteristics. The values of the asymptotic slopes for $B\gg1$ depend on the function $F(\theta)$.

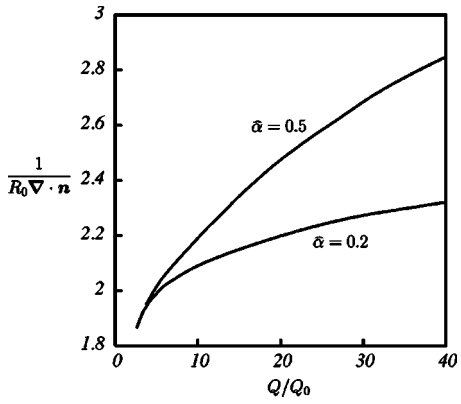

FIG. 7. Radius of curvature of the meniscus at the apex as a function of the flow rate for $\beta=0$ and two values of $\hat{\alpha}$.

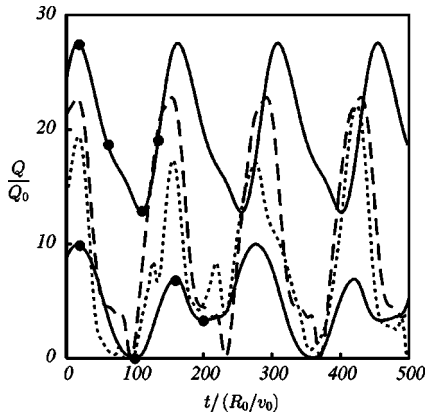

FIG. 8. Nondimensional evaporation flow rate (or current) as a function of the nondimensional time for $\hat{\alpha}=0.2$, $\beta=0$, and $(R_0/R_\infty)^2B=12.8$ (upper solid), 6.4 (dashed), 3.2 (dotted), and 0 (lower solid).

4. Oscillatory solutions

Not all the points of Fig. 2 correspond to stable solutions. On the lower curve ($\hat{\alpha}=0.2$, $\beta=0$), the transient solution of (6)–(12) does not settle to a stationary state when $(R_0/R_\infty)^2B$ is below the upper vertical mark of the figure. The unstable stationary solutions discussed above have been computed by subtracting a term proportional to $\boldsymbol{n}\cdot\nabla\phi-v_e$ from the right hand side of Eq. (11). This term amounts to an artificial damping force proportional to the normal speed of the surface, and therefore vanishes in the stationary state. When the artificial damping is suppressed, the solution of Eqs. (6)–(12) becomes oscillatory for values of $(R_0/R_\infty)^2B$ in the range between the two vertical marks of Fig. 2, and blows out after an oscillatory transient for values of this parameter below the lower mark.

Figure 8 shows the instantaneous current in the oscillatory regime as a function of time for different values of $(R_0/R_\infty)^2B$. As can be seen, the current is time periodic near the upper end of the range, and the amplitude of the oscillation increases and the shape of the wave becomes more complex when $(R_0/R_\infty)^2B$ approaches the lower end. The solution computed for $(R_0/R_\infty)^2B=1.6$ is not periodic, and the emission current switches off and on at irregular intervals. The current has undergone a period doubling when $B=0$.

The shape of the oscillatory meniscus is shown in Fig. 9 at four different instants during a cycle for $(R_0/R_\infty)^2B=12.8$ and 0. The keys 1–4 in each panel of Fig. 9 correspond to the times marked by black circles in Fig. 8, increasing with increasing time. As could have been expected, high instantaneous currents are attained when the elongation of the meniscus, and thus the harmonic field at its surface, is large. On the other hand, curve 2 of Fig. 9(b) (for $B=0$) shows that the meniscus is everywhere concave toward the liquid when the current is at its minimum and the evaporation is nearly quenched.

Increasing $\hat{\alpha}$ tends to stabilize the stationary solution, in line with the qualitative considerations of Sec. III B. The

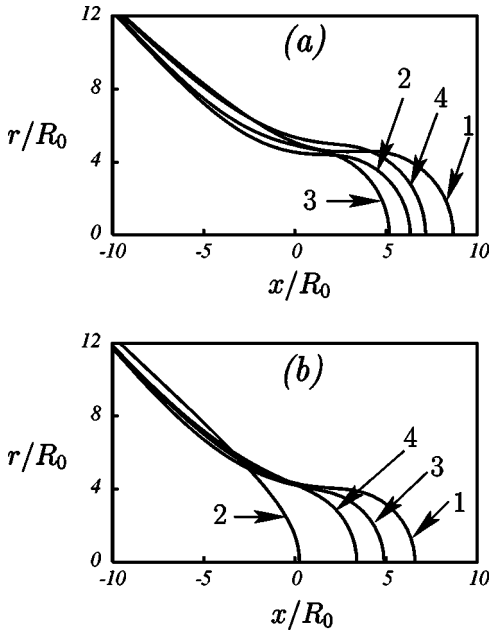

FIG. 9. Oscillatory tip of the meniscus at four different times during a period of the oscillation (keyed by black circles in Fig. 8) for $\hat{\alpha}=0.2$, $\beta=0$, and $(R_0/R_\infty)^2B=12.8$ (upper panel) and 0.

solution for $\hat{\alpha}=0.5$ (middle curve of Fig. 2) is already stable at low $(R_0/R_\infty)^2B$ all the way to extinction. Finally, oscillations have also been found for high values of $(R_0/R_\infty)^2B$; above about 32 when $\hat{\alpha}=0.2$ and 23 when $\hat{\alpha}=0.5$. These oscillations probably herald the "spraying mode" of LMIS's at high currents [4].

C. Asymptotic estimates for large values of *B*

The monotonous increase of Q/Q_0 with B for given $(\hat{\alpha},\beta)=O(1)$, and the monotonous evolution of the features of the flow, suggest that the solution is approaching an asymptotic regime for the largest values of B attained in the computations. An asymptotic structure of the solution can be proposed with the guide of these results and the experimental and theoretical results reviewed in the Introduction. The asymptotic structure should consist of a conical meniscus that prolongates into a narrow protrusion or neck whose length increases with the evaporating flow rate so as to keep a constant electric field equal to E_0 at its rounded end, where evaporation occurs. The scales of the evaporating cap and the neck can then be found using simple order of magnitude balances.

1. The evaporating cap

The stationary motion of the liquid leads to a depression via the Bernoulli equation $\frac{1}{2}\rho v^2+p=0$. At the surface of the cap, this depression is augmented by the inward stresses due to the evaporation recoil and the surface tension, and the sum of the three must be balanced by the outward electric stress $\frac{1}{2}\epsilon_0 E_0^2$. This condition limits the velocity of the liquid in the cap to values of the order of $v_0=\epsilon_0^{1/2}E_0/\rho^{1/2}$ at most. As a consequence, large flow rates can only be attained with large evaporation surfaces. The characteristic size of the cap, say R_c, should satisfy the order-of-magnitude relation $v_0R_c^2=Q$, whence $R_c=R_0(Q/Q_0)^{1/2}$, where the definitions of R_0 and Q_0 in Eq. (13) have been used.

On the other hand, the effect of the surface tension, which is inversely proportional to R_c and was of the order of the electric stress when the characteristic size of the evaporating surface was R_0 [see Eq. (13) and the discussion at the beginning of Sec. II B], becomes negligible in the balance of stresses at the cap when $Q/Q_0\gg 1$. The simplified balance reduces to $p+\frac{1}{2}\epsilon_0E_0^2=0$ in the particular case $\beta=0$, in which the velocity of the liquid is equal to v_0 at the surface.

2. The neck

The neck acts as a pipe for the liquid that evaporates at its downstream end. Calling x the axial distance measured from the join of the meniscus and the neck, and $r_s(x)$ the slowly varying radius of the neck, the velocity of the liquid will be $v\approx Q/\pi r_s^2$. The order-of-magnitude balance of flow-induced depression and electric stress discussed above also applies to the neck, where the surface field E_n is smaller than E_0. Using the Bernoulli equation and the expression of the velocity in the neck, the surface field that results from this balance can be written as

$$E_n=\frac{\rho^{1/2}Q}{\pi\epsilon_0^{1/2}r_s^2}. \tag{16}$$

This field is essentially radial and is due to the electric charge at the equipotential surface of the neck, which acts therefore as a line of charge of strength $\Phi(x)=2\pi r_s\epsilon_0E_n$ when seen from a distance large compared with r_s. It is not difficult to compute the axial field $E_{t_1}(x)$ induced by this distribution of charge at points of the neck surface. An approximation to this field which is correct only up logarithmic factors of the form $\ln(r_s/x)$ but that will be sufficient for the present purposes is $E_{t_1}(x)=(2\pi\epsilon_0)^{-1}d\Phi/dx$; see, e.g., Ref. [35]. Using the previous estimates of Φ and E_n, this approximation gives

$$E_{t_1}(x)=O\left(\frac{\rho^{1/2}Q}{\epsilon_0^{1/2}xr_s}\right) \tag{17}$$

in orders of magnitude.

Apart from the electric charge of the neck, there is additional surface charge at the conical meniscus. Since the surface of the liquid is an equipotential, the axial field $E_{t_1}(x)$ induced by the charge of the neck on itself has to be balanced by the axial field induced by the charge of the meniscus at the position of the neck, say $E_{t_2}(x)$. This field is not easy to compute because the distribution of charge of the meniscus is in turn affected by the presence of the neck. However, E_{t_2} can be estimated by noticing that the meniscus should tend to a Taylor cone at distances upstream of the neck of the order of its length (say ℓ_n). The field that a Taylor cone induces at distances of order ℓ_n downstream of its apex gives the estimate

$$E_{t_2}(\ell_n) = O[E_T(\ell_n)] = O\left(\frac{\gamma^{1/2}}{\epsilon_0^{1/2}\ell_n^{1/2}}\right), \tag{18}$$

where $\boldsymbol{E}_T = \boldsymbol{\nabla}\varphi_T$ is the field of Taylor's solution [1] [see also the paragraph following Eq. (11)].

Carrying the estimates (17) and (18) to the condition $E_{t_1} = E_{t_2}$, applied now for $x = O(\ell_n)$, and imposing, in addition, that E_n in Eq. (16) should satisfy $E_n(\ell_n) = O(E_0)$ in order to match with the evaporating cap, we find

$$\ell_n = O\left(\frac{\rho^{1/2}\epsilon_0^{1/2}E_0 Q}{\gamma}\right) = O\left(R_0\frac{Q}{Q_0}\right),$$

$$r_s(\ell_n) = O\left(\frac{\rho^{1/4}Q^{1/2}}{\epsilon_0^{1/4}E_0^{1/2}}\right) = O\left[R_0\left(\frac{Q}{Q_0}\right)^{1/2}\right].$$

Notice that $r_s(\ell_n)$ coincides with the estimate of the size of the cap R_c obtained in Sec. III C 1. The square root dependence of this magnitude on the flow rate is in line with the numerical results of Fig. 7 for large values of Q/Q_0.

The surface of the liquid ceases to be slender at the upstream end of the neck ($r_s \sim x$), and the condition that the surface tension should come back into play to match with the meniscus [$\gamma/r_s \sim \epsilon_0 E_n^2$ with E_n given by Eq. (16)] gives $(x, r_s) = O[R_0(Q/Q_0)^{2/3}]$ and $E = O[E_0/(Q/Q_0)^{1/3}]$.

3. $(Q/Q_0) - B$ relationship

The order of the voltage (as gauged by B) required to achieve a certain flow rate large compared with Q_0 can now be estimated. The electric potential at distances from the apparent apex of the Taylor cone large compared with ℓ_n should be of the form

$$\varphi_h(R', \theta') = A(\gamma/\epsilon_0)^{1/2}R'^{1/2}P_{1/2}(\cos\,\theta') + B'P_{-n}(\cos\,\theta')/R'^n + \cdots. \tag{19}$$

Here R' and θ' are spherical coordinates centered at the apparent apex, which needs not coincide with the center of the outer spherical electrode ($R = 0$) but will be displaced a certain distance δR from it. The leading term of Eq. (19) is the potential of Taylor's solution and the second term, with n an eigenvalue numerically close to $5/2$, comes from a straightforward linear analysis of the far field. The parameter B defined in Eq. (12a) appears when this $\varphi_h(R', \theta')$ is rewritten in terms of the original coordinates R and θ and the result is extrapolated to the outer electrode ($R = R_\infty \gg \delta R$). The first two terms of an expansion of $\varphi_h(R, \theta)$ in powers of $\delta R/R_\infty$ are $A(\gamma/\epsilon_0)^{1/2}R_\infty^{1/2}\{P_{1/2}(\cos\,\theta) - \frac{1}{2}(\delta R/R_\infty)P_{-1/2}(\cos\,\theta)\}$, where the first term coincides with the first term of φ_h in Eq. (12a) while the second term, along with higher order contributions from Eq. (19), should give the second term of φ_h in Eq. (12a). In orders of magnitude, this requires $\delta R = O[R_0(R_0/R_\infty)^2 B]$. If δR is assumed to be proportional to ℓ_n and the estimate of this magnitude worked out above is used, then $Q/Q_0 = O[(R_0/R_\infty)^2 B]$, in qualitative agreement with the approximately linear relation between Q/Q_0 and B displayed by the numerical results of Fig. 2 for $Q/Q_0 \gg 1$.

4. Additional comment

According to the estimates of this section, the effect of the surface tension is negligible around the tip when $Q/Q_0 \to \infty$. The results of Fig. 5 show that this is still not the case for the values of B used in the numerical computations (notice the tenfold magnification of the scale of the pressure in this figure), but they also suggest that the trend is for the depression to increase and eventually take over surface tension. Without an effect of the surface tension, the asymptotic solution is probably unstable, and the actual solution should not be expected to be stationary above a certain Q/Q_0 that may depend on $\hat{\alpha}$. All this is confirmed by the numerical results, but the asymptotic estimates are still useful because they reveal qualitative features of the stationary solution before it becomes unstable.

IV. CONCLUSIONS

Numerical computations and order-of-magnitude estimates have been used to describe the flow and the meniscus of a liquid ion source in a small region around its apex. The results rely on a simplified treatment of the space charge and the assumptions that the viscosity of the liquid and the electric field in the liquid are negligible. The model problem contains three nondimensional parameters that measure the strength of the flow and pressure variations induced in the liquid by ion evaporation, the recoil due to the momentum picked up by the evaporating flux of ions, and the voltage applied to the meniscus. In agreement with existing experimental and theoretical results, ion evaporation is seen to occur when the parameter that gauges the voltage is above a certain extinction value, and the evaporating surface is a cap at the end of a jetlike protrusion that the meniscus develops around its apex. The ionic current and the length of the protrusion increase linearly with the voltage. The size of the cap and the evaporation-induced depression also increase with the voltage. The effect of this depression is stabilizing; in its absence, the surface of the liquid either recedes until ion evaporation ceases or advances until a drop is shed. A time-dependent current is obtained in a certain range of voltages when the stabilizing effect of the depression is weak.

ACKNOWLEDGMENTS

This work has been supported by the Spanish Ministerio de Ciencia y Tecnología under Projects Nos. BFM2001-3860-C02-02 and DPI2002-4550-C07-5.

[1] G. I. Taylor, Proc. R. Soc. London, Ser. A **218**, 383 (1964).
[2] L. W. Swanson, Nucl. Instrum. Methods Phys. Res. **218**, 347 (1983); R. G. Forbes, Appl. Surf. Sci. **87**, 1 (1995).
[3] P. D. Prewett and G. L. R. Mair, *Focussed Ion Beams from LMIS* (Wiley, New York, 1991).
[4] R. G. Forbes, Vacuum **48**, 85 (1997).
[5] M. Gamero-Castaño and J. Fernández de la Mora, J. Chem. Phys. **113**, 815 (2000); M. Gamero-Castaño, Phys. Rev. Lett. **89**, 147602 (2002).
[6] J. V. Iribarne and B. A. Thomson, J. Chem. Phys. **64**, 2287 (1976).
[7] I. G. Loscertales and J. Fernández de la Mora, J. Chem. Phys. **103**, 5041 (1995); M. Gamero-Castaño and J. Fernández de la Mora, J. Mass Spectrom. **35**, 790 (2000); P. Kebarle, *ibid.* **35**, 804 (2000).
[8] I. Romero-Sanz, R. Bocanegra, J. Fernández de la Mora, and M. Gamero-Castaño, J. Appl. Phys. **94**, 3599 (2003); I. Romero-Sanz and J. Fernández de la Mora, J. Appl. Phys. **95**, 2123 (2004).
[9] K. L. Aitken, Eur. Space Agency, ESA SP **119**, 23 (1977).
[10] H. Gaubi, P. Sudraud, N. Tencé, and J. van de Walle, in *Proceedings of the 29th International Field Emission Symposium*, edited by H.-O. Anrén and H. Nordén (Almqvist and Wiskell, Stockholm, 1982), p. 357.
[11] G. Benassayag, P. Sudraud, and B. Jeffrey, Ultramicroscopy **16**, 1 (1985).
[12] D. R. Kingham and L. W. Swanson, Appl. Phys. A: Solids Surf. **A34**, 123 (1984).
[13] R. G. Forbes and N. N. Ljepojevic, Surf. Sci. **246**, 113 (1991); W. Liu and R. G. Forbes, Appl. Surf. Sci. **87/88**, 122 (1995).
[14] G. L. R. Mair, J. Phys. D **17**, 2323 (1984); G. L. R. Mair, Vacuum **36**, 847 (1986).
[15] G. L. R. Mair, Nucl. Instrum. Methods Phys. Res. B **88**, 435 (1994).
[16] R. G. Forbes, G. L. R. Mair, N. N. Ljepojevic, and W. Liu, Appl. Surf. Sci. **87**, 99 (1995).
[17] G. L. R. Mair and R. G. Forbes, J. Phys. D **24**, 2217 (1991); G. L. R. Mair and R. G. Forbes, Surf. Sci. **266**, 180 (1992).
[18] V. V. Vladimirov and V. N. Gorshkov, Appl. Phys. A: Solids Surf. **A46**, 131 (1988).
[19] G. L. R. Mair and A. von Engel, J. Appl. Phys. **50**, 5592 (1979).
[20] D. L. Bar and W . L. Brown, J. Vac. Sci. Technol. B **7**, 1806 (1989).
[21] B. Praprotnik, W. Driesel, Ch. Dietzsch, and N. Niedrig, Surf. Sci. **314**, 353 (1994).
[22] G. L. R. Mair, J. Phys. D **21**, 1654 (1988).
[23] V. V. Vladimirov, V. E. Badan, V. N. Gorshkov, L. G. Grechko, and A. Soloshenco, J. Vac. Sci. Technol. B **9**, 2582 (1991).
[24] C. Zheng and T. Linsu, J. Vac. Sci. Technol. B **6**, 2104 (1988).
[25] T. T. Tsong, Surf. Sci. **70**, 211 (1978); R. K. Biswas and R. G. Forbes, J. Phys. D **15**, 1323 (1982).
[26] T. E. Stern, B. S. Gossling, and R. H. Fowler, Proc. R. Soc. London, Ser. A **124**, 699 (1929).
[27] G. L. R. Mair, J. Phys. D **15**, 2523 (1982).
[28] J. P. Barbour, W. W. Dolan, J. K. Trolan, E. E. Martin, and W. P. Dyke, Phys. Rev. **92**, 45 (1953); J. W. Ward and R. L. Selinger, J. Vac. Sci. Technol. **19**, 1082 (1981).
[29] L. D. Landau and E. M. Lifshitz, *Electrodynamics of Continuous Media* (Pergamon, Oxford 1960).
[30] V. E. Krohn, J. Appl. Phys. **45**, 1144 (1974).
[31] G. K. Batchelor, *An Introduction to Fluid Dynamics* (Cambridge University Press, Cambridge, 1967).
[32] H. N. Oguz and A. Prosperetti, J. Fluid Mech. **257**, 111 (1993).
[33] P. K. Notz and O. A. Basaran, J. Colloid Interface Sci. **213**, 218 (1999).
[34] M. Cloupeau and B. Prunet-Foch, J. Aerosol Sci. **25**, 1021 (1994).
[35] H. Ashley and M. Landahl, *Aerodynamics of Wings and Bodies* (Addison-Wesley, Reading, 1965).